PCCP

PAPER

Cite this: *Phys. Chem. Chem. Phys.*, 2016, **18**, 5486

O_2 activation at the Au/MgO(001) interface boundary facilitates CO oxidation†

Zhiyao Duan and Graeme Henkelman*

Received 17th September 2015,
Accepted 5th January 2016

DOI: 10.1039/c5cp05558j

www.rsc.org/pccp

Density functional theory calculations reveal that the work function of Au supported on MgO(001) is substantially reduced because of an interfacial dipole moment formed at the Au/MgO interface. Consequently, the Au/MgO interface plays an active role in the activation of O_2 molecules by promoting charge transfer to the O_2 $2\pi^*$ orbital. The presence of F-centers in the MgO substrate can further promote the charge transfer and bonding of O_2 at the interface boundary. However, O_2 dissociation is kinetically hindered. The system is then able to catalyze CO oxidation at low temperature as adsorbed CO and O_2 readily react to form CO_2 with a low energy barrier.

1 Introduction

Metal oxide supported Au catalysts are highly active for CO oxidation at low temperature.[1–5] This catalytic behavior is surprising in that the components, bulk Au and the oxide support, are inert for CO oxidation. Since it is generally accepted that CO can readily adsorb on the surface of the Au nanoparticles (Au NPs),[6] it is believed that O_2 activation is the crucial step in the oxidation reaction. Depending on the nature of the oxide support (reducible *vs.* non-reducible, defect-free *vs.* defect-rich, and surface orientation, *etc.*) and the size of Au NPs, the active sites for O_2 activation can vary. Proposed active sites for O_2 activation include, but are not limited to, under-coordinated Au atoms on small Au clusters,[7] perimeter sites at the Au/oxide interface,[8–10] and surface lattice oxygen vacancies (the redox pathway).[4,11]

Relevant to the system of Au supported on MgO surface under investigation here, experiments on Au_n $(2 \leq n \leq 20)$ soft-landed on MgO(001) thin film showed that CO_2 production is greatly enhanced for Au clusters on defect rich films as compared to Au clusters on defect poor films.[12] Supporting quantum chemistry calculations revealed that F-centers on MgO induce a partial electron transfer to the Au_8 cluster, which enhances the O_2 binding energy and activates the O–O bond to a peroxo-like adsorbate state. A recent theoretical study using global optimization pointed out that the supported Au_8 cluster can transform into a shape favorable for O_2 adsorption, leading to an lower effective O_2 binding energy.[13] The critical role of the F-center in the activation of Au in Au/MgO catalysts was also confirmed on larger supported Au NPs, in the size range of 3.8–4.3 nm.[14] From the above studies, the role of F-centers is shown to be important in O_2 activation, but some questions remain about the mechanism of O_2 activation: is the defect-free Au/MgO interface capable of activating O_2? What has changed when F-centers are present at the interface? Previous computational studies on this topic found that O_2 can only be activated when co-adsorbed with CO at the interface forming a metastable $CO{\cdot}O_2$ peroxo-like intermediate.[15,16] However, O_2 adsorption at the interface was shown to be unfavorable (only 0.2 eV with respect to a gas-phase oxygen molecule), so that it is questionable if the probability of forming the $CO{\cdot}O_2$ intermediate would be high enough to sustain CO oxidation reactivity.

In this work, to address the role of Au/MgO interface in O_2 activation, we present a theoretical study using density functional theory (DFT). We demonstrate that the Au/MgO interface creates an interfacial dipole that is responsible for a substantial decrease of the Au work function. The change in work function promotes an electron transfer to the $2\pi^*$ orbital of O_2, which enhances the O–O bond activation. The presence of a surface F-center can further enhance the O_2 activation by transferring more charge to the $2\pi^*$ orbital.

2 Computational details

Plane-wave based DFT calculations were performed using the Vienna *Ab initio* Simulation Package.[17–19] All calculations considered spin-polarization. The energy cutoff of the plane-wave basis was set to 400 eV. The generalized gradient approximation with the Perdew–Wang (GGA-PW91) functional[20] was used to describe the exchange and correlation energy. Electron–ion interactions were treated by the projector augmented wave method.[21] Due to the large model employed, a single Γ point sampling of the

Department of Chemistry and the Institute for Computational Engineering and Sciences, The University of Texas at Austin, Austin, TX 78712-0165, USA.
E-mail: henkelman@utexas.edu; Fax: +1 512 471 8696; Tel: +1 512 471 4170

† Electronic supplementary information (ESI) available: Additional binding energies, geometries, and reaction pathways. See DOI: 10.1039/c5cp05558j

Brillouin zone was used to calculate the total energy of the system. Optimized structures were obtained by minimizing the forces on each ion until they fell below 0.05 eV $Å^{-1}$. Transition states were determined with the climbing image nudged elastic band method.[22,23] A Bader analysis was employed to determine the local charge of atoms in the system.[24–26] The dipole induced by the asymmetric slab model is compensated for by adding a linear electrostatic potential to the local potential. The local potential then has two different values on the two surfaces of the slab. The vacuum electrostatic potential level corresponding to the lower surface of the Au rod in contact with the support is used as the energy reference to calculate the work function of Au.

A full atomic model of the 2–3 nm supported Au nanoparticles investigated experimentally is prohibitively large to simulate with DFT calculations. Instead only the Au/MgO interface boundary, that is the most catalytically relevant, is considered. Our model consists of a Au rod placed on the surface of the MgO(001) slab. The MgO(001) slab contains four layers with the bottom two layers fixed to bulk positions. For the Au rod, the Au(111) surface is chosen as facing the MgO(001) surface. Recent theoretical calculations justify this choice, showing that the FCC(111) orientation is energetically more stable than the FCC(001) orientation, when the Au nanoparticle is over 1000 atoms.[27] Two interface boundary directions, denoted as Au‖MgO[110] and Au‖MgO[100], are considered, as shown in Fig. 1. Based on the calculated lattice constants of Au (4.207 Å) and MgO (4.238 Å), the Au rod is strained by +1.6% and −4.1% to match the lengths of the MgO slabs along the MgO[110] and MgO[100] directions, respectively. The Au rod aligned along the MgO[110] direction can sit atop either Mg or O rows. In our calculation, the Au rod siting atop O rows is 0.5 eV more stable than atop Mg rows. When aligned along the MgO[100] direction, the Au boundary atoms are in contact with alternating Mg and O atoms.

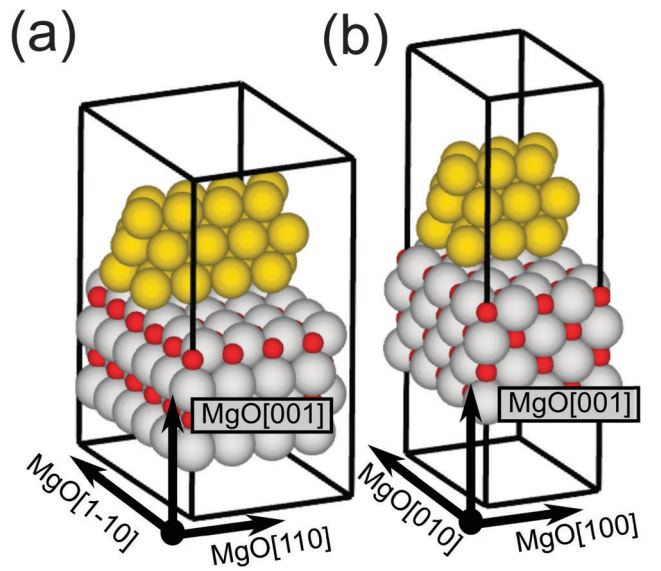

Fig. 1 Perspective views of our models for Au rods supported on MgO(001): (a) along the MgO[110] direction and (b) along the MgO[100] direction. The atoms are colored as: grey (Mg), red (O), and yellow (Au).

Accordingly, we found no noticeable energy difference as a result of shifting the Au rod along the [010] direction. After relaxing the above described models, the distances between the Au rod and the MgO slab were determined to be 3.05 Å and 2.96 Å for the Au‖MgO[110] and Au‖MgO[100] models, respectively. This distance, from a recent scanning transmission electron microscopy study, was measured as 3.07 ± 0.11 Å, which is in excellent agreement with our calculations.[28]

3 Result and discussion

3.1 Electronic structure of the Au/MgO interface

The electronic structure of the Au/MgO interface is first studied to reveal the synergistic effect between the Au and MgO components. The PDOS of the Au rod and the MgO substrate before and after interface formation are shown in Fig. 2(a), where the energy of the electronic states are referenced to the electrostatic potential at the center of the vacuum layer. The work function of the Au rod decreases significantly by 1.23 eV which can be attributed to the interfacial dipole moment. The dipole can be visualized from the charge density difference ($\Delta\rho = \rho_{Au/MgO} - \rho_{Au} - \rho_{MgO}$) when Au is supported on MgO, as plotted in Fig. 2(b). There, a negative charge layer is close to the interfacial Au atoms residing atop Mg cations and a positive charge layer is above O anions. The reorganization of charge at the interface has been previously explained by two effects, charge transfer across the interface and polarization of metallic electron cloud induced by the oxide substrate.[29–31] Quantitatively, the interfacial dipole moment normal to the surface, $\Delta\mu = \int_{-\Delta z}^{\Delta z} z\Delta\rho_z dz$, where Δz is the integration distance with respect to the center of the interface, is calculated to be −0.28 D. The direction of the calculated $\Delta\mu$ is in consistent with the reduced work function.

3.2 O_2 adsorption

As a result of the reduction in the Au work function, the unoccupied $2\pi^*$ orbital of O_2, which was previously positioned above the unsupported Au Fermi energy, becomes lower than the Fermi energy of supported Au on MgO, as shown in

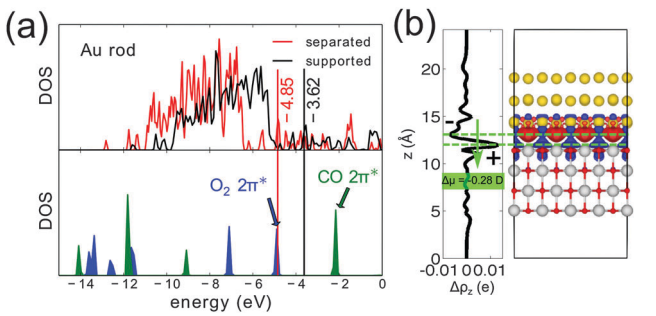

Fig. 2 (a) Projected density of states (PDOS) of the Au rod and the MgO substrate before and after the Au rod is supported on the MgO substrate. The charge redistribution due to the interface formation ($\Delta\rho$) is shown in (b), where red indicates electron gain and blue indicates electron depletion. The *xy*-plane averaged $\Delta\rho$ is also shown in (b) to show the interfacial dipole.

Table 1 Adsorption energies, bond lengths, charge and dissociation barrier of O_2 and CO adsorbed at the Au/MgO interface boundary; numbers in parenthesis are for the unsupported Au rod

	Strain (%)					
Model	Au rod	MgO slab	$E_{O_2}^{ads}$ (eV)	d_{O-O} (Å)	Charge (e)	E_a (eV)
Au‖MgO[110]	+1.6	0.0	−0.89 (−0.55)	1.400 (1.339)	−0.87 (−0.56)	1.2
Au‖MgO[100]	−4.1	0.0	−0.19 (−0.01)	1.359 (1.272)	−0.73 (−0.24)	
Au‖F-MgO[110]	+1.6	0.0	−1.04 (−0.55)	1.411 (1.339)	−0.93 (−0.56)	1.1

	Strain (%)					
Model	Au rod	MgO slab	E_{CO}^{ads} (eV)	d_{C-O} (Å)	Charge (e)	E_a (eV)
Au‖MgO[110]	+1.6	0.0	−0.67 (−0.65)	1.181 (1.178)	−0.20 (−0.15)	
Au‖MgO[100]	−4.1	0.0	−0.41 (−0.56)	1.170 (1.167)	−0.18 (−0.08)	

Fig. 2(a). Electron transfer from the interface to the 2π* orbital is then expected. A Bader charge density analysis confirms the charge transfer to O_2 at the interface boundary, as summarized in Table 1. At the Au‖MgO[110] boundary, adsorbed O_2 is charged by −0.87 e, which is −0.31 e more than on the unsupported Au rod. The charge transfer is also evident at the Au‖MgO[100] boundary. The atomic structure and the charge difference plot ($\Delta\rho = \rho_{O_2/Au/MgO} - \rho_{Au/MgO} - \rho_{O_2}$) of adsorbed O_2 at the Au‖MgO[110] and Au‖MgO[100] boundaries are shown in Fig. 3. The charge density difference plots clearly reveal the enhanced charging of the 2π* orbital from the interface. The activation of O_2 at the interface boundary is also apparent from structural properties. The O–O bond length (Table 1) is elongated by 0.06 Å and by 0.08 Å when adsorbed at Au‖MgO[110] and Au‖MgO[100] boundaries, respectively. O_2 binding strength is therefore enhanced at the interface boundary because the charge transfer to O_2 relieves the high energy of the interfacial electrons. The charge transfer and O_2 activation at the interface boundary is relatively insensitive to the strain in the Au rod, as demonstrated in Table S2 of the ESI.† The binding energy of O_2, however, does vary with strain as anticipated by the d-band theory.[32] The enhanced O_2 activation is only observed at the interfacial Au layer; when O_2 is absorbed on Au atoms away from the interface, the binding energy remains the same as compared to the unsupported Au rod (see Table S1 in the ESI†).

The binding of O_2 is more pronounced at the Au‖MgO[110] boundary than at the Au‖MgO[100] boundary. The difference is due to the fact that the adsorbed O_2 at the Au‖MgO[100] boundary is close to a surface O anion, which induces a repulsive force to the charged O_2. In contrast, the Au‖MgO[110] boundary consists of Mg cations, which stabilize the charged O_2 by an attractive electrostatic interaction.

While the O_2 dissociation at the interface boundary is exothermic by 0.49 eV, the barrier is calculated to be 1.2 eV so that O_2 dissociation is kinetically unfavorable. The minimum energy path for O_2 dissociation is shown in Fig. 1 in the ESI.† Molecular beam experiments on 1.5 nm Au NPs showed that, after exposure to O_2, no CO_2 was produced during CO titration, indicating that O_2 does not dissociate on Au NPs.[33]

To examine the influence of an F-center on O_2 adsorption, an oxygen vacancy is introduced into the Au/MgO interface. The F-center is placed directly under the center of the Au rod and cannot be accessed at the interface boundary. When an F-center is present at the interface, the Au work function reduction is further enhanced; the Au Fermi energy is raised from −4.84 to −3.05 eV (Fig. 4(a)). The charge density difference plot, in Fig. 4(b), shows the electron transfer from the F-center to the interfacial Au layer. The larger interfacial dipole moment is consistent with the Au work function reduction. The O_2 binding energy is calculated to be −1.03 eV, which is −0.14 eV lower than without the F-center. The energy barrier of O_2 dissociation at the defected interface is calculated to be 1.1 eV. The MEP of this process is shown in Fig. S2 in the ESI.† Although it is a little lower than the barrier at the stoichiometric interface, the dissociation process is still kinetically limited at low temperature.

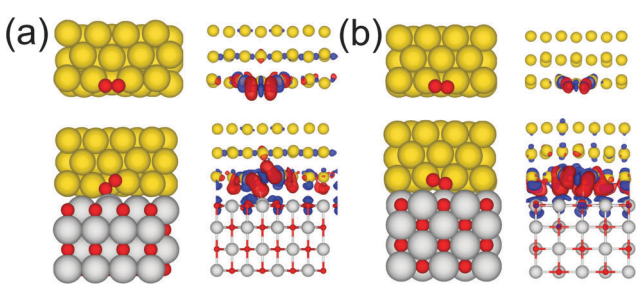

Fig. 3 Relaxed structures of O_2 adsorbed on the isolated Au rod and at the Au/MgO interface boundary along the (a) MgO[110] and (b) MgO[100] directions. The charge difference upon O_2 adsorption is also shown.

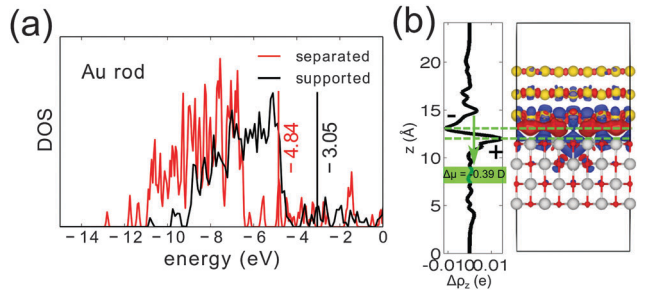

Fig. 4 (a) PDOS of the Au rod and MgO substrate with an F-center before and after the Au rod is supported. The energy reference is the vacuum level. (b) Charge redistribution due to interface formation.

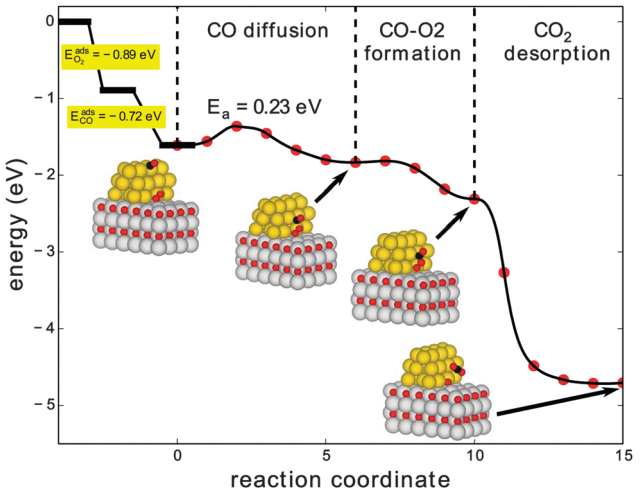

Fig. 5 Minimum energy path for CO oxidation at the Au/MgO interface boundary. The red points correspond to the actual images used in the NEB calculations; the curve is the result of a force-based interpolation between the images.

Unlike O_2, C–O bond activation is not promoted at the Au/MgO interface boundary (Table 1). The reason is that the CO $2\pi^*$ orbital remains above the Fermi level of the Au/MgO interface.

3.3 CO oxidation

It is clear that O_2 adsorption is preferred over CO adsorption at the Au/MgO interface. Following this result, a CO oxidation mechanism is proposed, as shown in Fig. 5. First, the CO is adsorbed at the edge of the Au rod and O_2 is adsorbed at the Au/MgO interface with adsorption energies −0.72 and −0.89 eV, respectively. Then the adsorbed CO diffuses toward the adsorbed O_2 at the interface boundary. CO diffusion is the most activated elementary step, with an energy barrier of 0.23 eV. An activated $CO{\cdot}O_2$ complex is formed and the O–O bond is further weakened. The formation of the $CO{\cdot}O_2$ intermediate is energetically favorable as compared to separately adsorbed CO and O_2, by about 0.5 eV. Finally, CO_2 is desorbed from the $CO{\cdot}O_2$ complex without a barrier and a reaction energy of 2.3 eV. The F-center located at the interface decreases the binding energy of O_2 and increases the availability of O_2 at the interface. The remaining adsorbed O is highly active; there is no barrier for it to react with a second CO.

It should be noted that the aforementioned energetics of CO oxidation is calculated with a tensile strained Au rod. Since the O_2 adsorption energy strongly depends on strain in the Au support, which is not well-known experimentally, the preferential binding of O_2 over CO at the interface can be weakened or even reversed depending on the actual strain in the Au rod.

4 Conclusion

In summary, we have demonstrated that the Au work function is significantly reduced when supported on MgO. At the interface, charge transfer to the O_2 $2\pi^*$ is enhanced, which facilitates activation of the O–O bond. The Au/MgO boundary along the MgO[110] direction binds O_2 stronger than the MgO[100] direction. The presence of F-centers also lead to enhanced O_2 binding. As a result of this O_2 activation, the system is predicted to be active for CO oxidation.

Acknowledgements

This work is supported by the Department of Energy under contract DE-FG02-13ER16428 and the Welch Foundation under grant F-1841. The calculations were done at the National Energy Research Scientific Computing Center and the Texas Advanced Computing Center.

References

1 M. Haruta, T. Kobayashi, H. Sano and N. Yamada, *Chem. Lett.*, 1987, 405–408.
2 M. Haruta, N. Yamada, T. Kobayashi and S. Iijima, *J. Catal.*, 1989, **115**, 301–309.
3 M. Haruta, *CATTECH*, 2002, **6**, 102–115.
4 G. C. Bond and D. T. Thompson, *Gold Bull.*, 2000, **33**, 41–50.
5 R. Meyer, C. Lemire, S. Shaikhutdinov and H.-J. Freund, *Gold Bull.*, 2004, **37**, 72–124.
6 K. Christmann, S. Schwede, S. Schubert and W. Kudernatsch, *ChemPhysChem*, 2010, **11**, 1344–1363.
7 N. Lopez, T. Janssens, B. Clausen, Y. Xu, M. Mavrikakis, T. Bligaard and J. K. Nørskov, *J. Catal.*, 2004, **223**, 232–235.
8 D. Widmann and R. J. Behm, *Angew. Chem., Int. Ed.*, 2011, **50**, 10241–10245.
9 Y. Y. Wu, N. A. Mashayekhi and H. H. Kung, *Catal. Sci. Technol.*, 2013, **3**, 2881–2891.
10 Z. Duan and G. Henkelman, *ACS Catal.*, 2015, **5**, 1589–1595.
11 L. Li, A. Wang, B. Qiao, J. Lin, Y. Huang, X. Wang and T. Zhang, *J. Catal.*, 2013, **299**, 90–100.
12 A. Sanchez, S. Abbet, U. Heiz, W.-D. Schneider, H. Hkkinen, R. N. Barnett and U. Landman, *J. Phys. Chem. A*, 1999, **103**, 9573–9578.
13 L. B. Vilhelmsen and B. Hammer, *Phys. Rev. Lett.*, 2012, **108**, 126101.
14 Z. Yan, S. Chinta, A. A. Mohamed, J. P. Fackler and D. W. Goodman, *J. Am. Chem. Soc.*, 2005, **127**, 1604–1605.
15 L. M. Molina and B. Hammer, *Phys. Rev. Lett.*, 2003, **90**, 206102.
16 L. M. Molina and B. Hammer, *Phys. Rev. B: Condens. Matter Mater. Phys.*, 2004, **69**, 155424.
17 G. Kresse and J. Hafner, *Phys. Rev. B: Condens. Matter Mater. Phys.*, 1993, **47**, 558.
18 G. Kresse and J. Furthmüller, *Comput. Mater. Sci.*, 1996, **6**, 15–50.
19 G. Kresse and J. Furthmüller, *Phys. Rev. B: Condens. Matter Mater. Phys.*, 1996, **54**, 11169.
20 J. P. Perdew and Y. Wang, *Phys. Rev. B: Condens. Matter Mater. Phys.*, 1992, **45**, 13244.
21 P. E. Blöchl, *Phys. Rev. B: Condens. Matter Mater. Phys.*, 1994, **50**, 17953.
22 G. Henkelman and H. Jónsson, *J. Chem. Phys.*, 2000, **113**, 9978–9985.

23 G. Henkelman, B. P. Uberuaga and H. Jónsson, *J. Chem. Phys.*, 2000, **113**, 9901–9904.
24 R. F. W. Bader, *Atoms in Molecules: A Quantum Theory*, Oxford University Press, New York, 1990.
25 G. Henkelman, A. Arnaldsson and H. Jónsson, *Comput. Mater. Sci.*, 2006, **36**, 354–360.
26 W. Tang, E. Sanville and G. Henkelman, *J. Phys.: Condens. Matter*, 2009, **21**, 084204.
27 R. Ferrando, G. Rossi, A. C. Levi, Z. Kuntová, F. Nita, A. Jelea, C. Mottet, G. Barcaro, A. Fortunelli and J. Goniakowski, *J. Chem. Phys.*, 2009, **130**, 174702.
28 Y. Han, R. Ferrando and Z. Y. Li, *J. Phys. Chem. Lett.*, 2014, **5**, 131–137.
29 L. Giordano, F. Cinquini and G. Pacchioni, *Phys. Rev. B: Condens. Matter Mater. Phys.*, 2006, **73**, 045414.
30 S. Prada, U. Martinez and G. Pacchioni, *Phys. Rev. B: Condens. Matter Mater. Phys.*, 2008, **78**, 235423.
31 J. Goniakowski and C. Noguera, *Inter. Sci.*, 2004, **12**, 93–103.
32 M. Mavrikakis, B. Hammer and J. K. Nørskov, *Phys. Rev. Lett.*, 1998, **81**, 2819–2822.
33 O. Meerson, G. Sitja and C. R. Henry, *Eur. Phys. J. D*, 2005, **34**, 119–124.

